



SEISMIC ANALYSIS OF THE NEW TACOMA NARROWS SUSPENSION BRIDGE

Michael JONES¹, Semyon TREYGER² and Patrick PENCE³

SUMMARY

This paper presents the seismic analysis that was conducted for the new Tacoma Narrows Suspension Bridge, which is located in the Seattle-Tacoma area of the State of Washington. This area is in a high seismicity region, capable of producing earthquakes of Richter moment magnitude eight or larger. Project specific performance-based design criteria mandated that a non-linear time-history analysis be used to supply the bridge with prescribed levels of seismic resistance. Some of the analysis subjects discussed include damping, soil-structure interaction, caisson rocking, hydrodynamic mass, and finite element modeling of various bridge components. The paper demonstrates that analysis techniques are available to confirm that seismic goals specified by performance-based design criteria are achievable for bridges in high seismic regions.

INTRODUCTION

In June, 1993, the Washington State Legislature unanimously enacted the Public/Private Initiatives Act to attract private business investment for un-funded State transportation needs. The new Tacoma Narrows Suspension Bridge, now under construction, was a direct consequence of this initiative. Since transportation capacity improvements across the Tacoma Narrows had been the focus of intensive studies during the last two decades, the Washington Department of Transportation (WSDOT) evaluated proposed solutions and alternatives, including adding a lower roadway to the existing bridge or the construction of a new parallel bridge. After evaluating these alternatives, WSDOT issued a Notice-to-Proceed (NTP) on September 25, 2002 for a design-build agreement to construct a new parallel bridge. A computer rendering of the new bridge is shown in Figure 1.

The new Tacoma Narrows Suspension Bridge will significantly increase the capacity of SR 16 between the Seattle-Tacoma metropolitan area and the Olympic Peninsula, by providing separate bridges for traffic in each direction. The \$680,000-million, design-build agreement, includes both the construction of the new bridge and the seismic retrofit of the existing bridge and construction of all approaches. When completed, the new bridge will be the first major suspension bridge in the world to be constructed under a design-build delivery method, as well as the longest span built in the United States since the Verezano-Narrows Bridge was completed in 1964. The new suspension bridge will consist of an 853.7 m (2800 ft) main span supported by reinforced concrete towers. The towers will be founded on massive gravity caissons of open-dredge construction. Gravity anchorages on the hillsides of the Narrows will secure the

¹Project Manager, HNTB Corporation, Santa Ana, USA. Email: mjones@hntb.com

²Associate Vice President, HNTB Corporation, Seattle, USA. Email: streyger@hntb.com

³Senior Project Engineer, HNTB Corporation, Santa Ana, USA. Email: ppence@hntb.com

main suspension cables. A unique orthotropic deck system will be integral with the superstructure truss, and the design will identify necessary provisions for a future lower deck to support additional traffic and the future possibly of a light rail system. The project schedule includes a fast-track design which will accommodate the project delivery schedule of 55 months.



Figure 1 – New Tacoma Narrows Suspension Bridge, shown to the left of the existing bridge

PERFORMANCE-BASED DESIGN CRITERIA

Contract documents provided performance-based design criteria (Criteria). The principle design code referenced by Criteria was the WSDOT Bridge Design Manual [1]. Criteria stipulated that the structure must comply with specified performance levels for two distinct seismic levels. The upper seismic level, referred to as the Safety Evaluation Earthquake (SEE), was defined as a seismic event with a mean return period of 2,500 years. The lower seismic level had a mean return period of 100 years, and was designated the Functional Evaluation Earthquake (FEE). Criteria also specified that three unique ground motion records should be used during time-history analysis for the SEE. Each of these records was further specified to have three orthogonal components, two horizontal and one vertical. Only one three-component ground motion was required for the FEE. Because of the large distance between foundation elements, consideration of ground motion spatial incoherency was also required. Criteria further specified that all non-linear analysis be performed with the ADINA [2] general purpose finite element software. Table 1 summarizes key components of the performance-based design criteria.

Table 1 – Performance-Based Design Criteria Summary

Component	Seismic Event Level					
	SEE			FEE		
	Maximum Material Strain		Residual Drift	Maximum Material Strain		Residual Drift
	Conc.	Steel		Conc.	Steel	
Caissons	(1)	(1)	12" in any direction	0.004	0.015	None Permitted
Anchorage Blocks	(2)	(2)	12" Longitudinal, 6" Transverse	0.004	0.015	None Permitted
Towers	0.75 ϵ_u (7)	0.05 ³	Longitudinal: 12" at top, 24" between tower top and bottom Transverse: 36" Top, 24" between top and bottom	0.004	0.015	None Permitted
Stiffening Truss - Primary Member	-	(2)	None Permitted	-	(6)	None Permitted
Stiffening Truss - Secondary Member	-	(4)	Permanent deformations associated with allowable damage	-	(6)	None Permitted
Cable System	-	(5)	None Permitted	-	(6)	None Permitted
Expansion Joints	-	-	Significant Damage Allowed	-	(6)	None Permitted

¹Strains not specified. Minimal damage with minor inelastic yielding permitted.
²Strains not specified. Force Demand/Capacity (D/C) ratio of not greater than 1.0.
³Steel strain of 0.05 permitted for tower #36 (#11) longitudinal bars and #16 (#5) confining reinforcement.
⁴Strains not specified. Force Demand/Capacity (D/C) ratio of not greater than 1.5.
⁵Load capacity of suspenders taken as half of the ultimate breaking strength. Stress of 760 MPa (110 ksi) permitted for suspension cable.
⁶Strains not specified. Elastic performance required with no damage permitted.
⁷ ϵ_u is the ultimate confined concrete strain.

CAISSON MODELING

A typical cross-section of the dredged caisson is shown in Figure 2. Caissons were modeled with elastic beam elements. Figure 3 provides a view of a typical caisson ADINA model. The gross moment of inertia was used for member stiffness based on the assumption that the size of the caisson is large relative to caisson seismic demands. Since the plan size of caissons, 24.4 m (80 ft) by 39.6 m (130 ft), is quite large relative to the “stick” beam element used to represent caissons (see Figure 3), the rotation mass moment of inertia along three orthogonal axes were lumped at each node. Hydrodynamic mass, representing water surrounding the perimeter of the caissons that participates in seismic loading, was estimated by a procedure published by Goyal and Chopra [3], and lumped at each node of the caissons between the mudline and the ocean surface. Since dredge wells are completely filled with water and sloshing cannot occur, the water within the dredge wells was assumed to fully participate in seismic re-

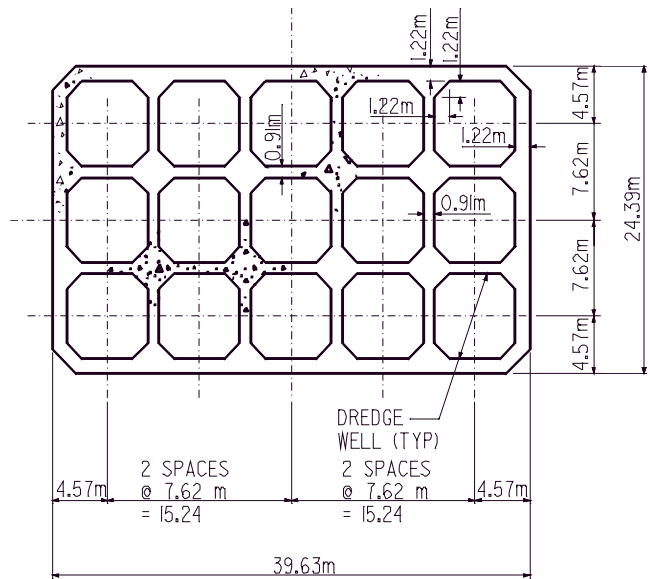


Figure 2 – Dredged caisson cross-section

sponse. In the two orthogonal horizontal directions, dredge well water was lumped at each node along the length of dredge wells based on tributary volume. In the vertical direction, the total mass of dredge water was lumped entirely at the node representing the top of the caisson seal slab, located 7.62 m (25 ft) above the bottom of the caisson. The full density of concrete was used for caisson members, including submerged portions of the caissons. Hydrostatic buoyancy caisson force was assumed to remain constant throughout seismic events and was applied at the bottom of the caisson. When determining buoyancy forces, a constant sea level of +0.76 m (2.5 ft) was assumed for all seismic events.

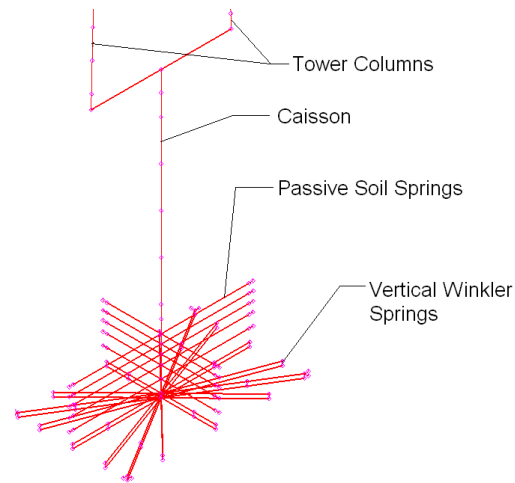


Figure 3 – ADINA model at caisson

CAISSON SOIL-STRUCTURE INTERACTION

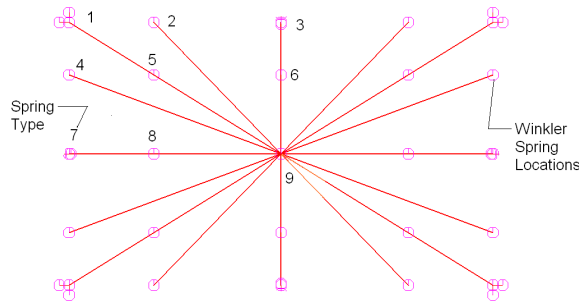


Figure 4 – Winkler soil spring locations at bottom of caissons

A number of non-linear modeling techniques were required to capture soil-structure interaction, permit caisson rocking, and to help provide an indication of caisson residual drift. Soil support at the bottom of the caisson was captured through twenty-five (25) truss elements modeled with a non-linear plastic material model. These non-linear Winkler soil springs were configured in a “spider net” configuration as shown in Figure 4. Table 2 provides the area distribution represented by each spring type. An intentional effort was made to place more springs toward the perimeter of the caisson, since caisson rocking effects on supporting soil would be greatest away from the caisson center. Sensitivity studies indicated that discretization schemes with less than 25 springs did not provide sufficient accuracy, while the additional refinement provided by a finer mesh was not warranted. Results from one such comparison with a stand-alone caisson model using 169 equally-spaced springs is shown in Figure 5. Note the good correlation between the 25-spring and 169-spring models.

Table 2 – Area Distribution of Winkler Soil Springs At Bottom of Caisson

Spring Type (Figure 4)	Tributary Area (m ²)	Percent of Total
1	9.66	1.0
2	19.32	2.0
3	38.65	4.0
4	19.32	2.0
5	38.65	4.0
6	77.30	8.0
7	38.65	4.0
8	77.30	8.0
9	154.6	16.0

Winkler soil springs are attached to the bottom of caissons through parallel sets of rigid links, as shown in Figure 3. One set of rigid links is attached to the bottom of the caisson, while the other set is attached to a single ground node directly below the caisson. Using this arrangement minimized the number of ground nodes required to impart ground motions to the structure. Winkler soil spring elements only permit compression loading and allow the development of gaps between soil and the caisson bottom during caisson rocking. The geotechnical engineer supplied non-linear force-displacement curves of

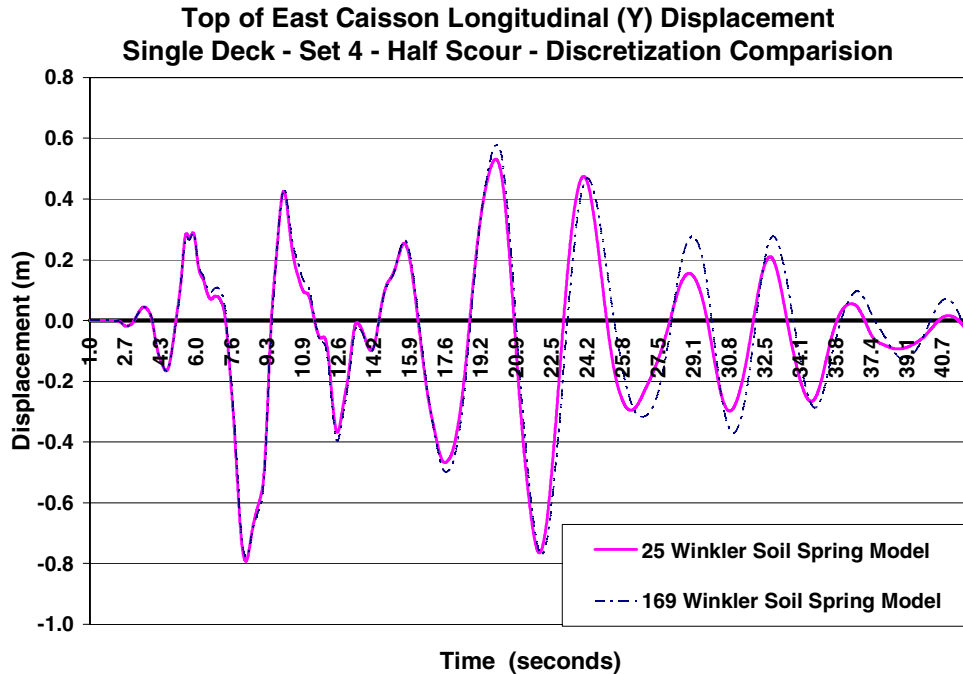


Figure 5 – Comparison of longitudinal displacements at top of East Caisson with two different Winkler soil spring discretization schemes below caissons

supporting soil, which were used to develop the caisson soil springs. These springs were developed through full soil-structure continuum models developed by the geotechnical engineer, Lam [4]. Characteristics of a typical force-displacement curve are shown in Figure 6. These force-displacement curves consider both the location of each soil spring relative to the caisson bottom as well as the area supported by the spring. The initial slope of the soil force-displacement curve represents the elastic response of supporting soil. Subsequent branches of the force-displacement curve represent plastic deformation of the soil. The material model adopted to represent soil force-displacement curves permits strain hardening once the elastic capacity of the soil is exceeded. After strain hardening, the initial elastic slope of the force-displacement curve is always followed during subsequent loading cycles. Since material models cannot support tension stresses, soil gaps will form after unloading once the elastic limit of truss elements is exceeded. This modeling technique was selected due to the ability to provide an estimate of residual displacements of caissons at the end of a seismic event. This modeling technique also captures increased soil damping as a consequence of rocking and plastic deformation of supporting soils through the hysteretic damping provided by the non-linear plastic material model.

It is recognized that the soil model represented by Figure 6 is an approximation of the actual soil response and was chosen primarily as a convenient modeling tool for implementation into global finite element models. This modeling technique fails to capture many soil parameters such as three-dimensional and confining stress effects. However, even with these limitations, results were compared to full stand-alone caisson models with the soil modeled as a full continuum and very good agreement was found between caisson displacements and forces Lam [5].

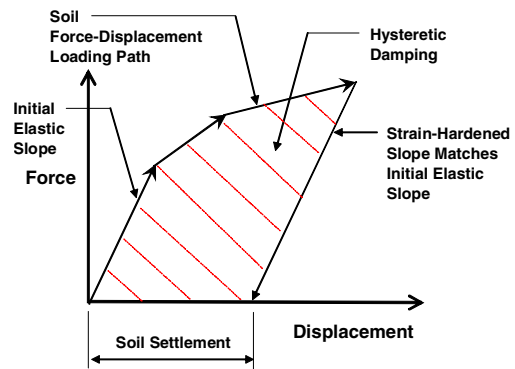


Figure 6 – Non-linear Winkler soil spring force-displacement plot

Passive soil resistance along the sides of the caisson below the mudline was also captured with non-linear Winkler soil springs. These springs have similar characteristics to the vertical soil springs used and permit soil gapping at caisson sides when caissons move away from supporting soil. As previously seen in Figure 3, passive resistance is lumped at the center of each face of the caisson. In addition to horizontal passive resistance, additional and significant horizontal soil support is provided by traction springs placed at the bottom of the caissons. These springs incorporate the large sliding resistance provided by friction at the base of the caissons. To provide caisson torsion stability, pairs of traction springs were placed at each corner of caissons, which continually engage the caisson corners, regardless of the level of uplift experienced at the caisson base. Non-linear plastic material models were also used to model traction springs, but tension gapping was not allowed, which resulted in tractions springs resisting sliding in both directions. Seismic input ground motions were introduced into the model through the Winkler soil springs located at the bottom and sides of caissons. In addition, ground motion variation along the length of caissons (deconvolution analysis) was performed by the geotechnical engineer.

TOWER MODELING

A discretization plan of the west tower is shown in Figure 7, with Figure 8 providing a cross-section of the tower column. Towers are composed of two rectangular hollow concrete columns and three hollow rectangular struts. The tower columns are constructed with 0.61 m (2.0 ft) thick walls, except from the upper deck level down to the caisson where thickness is increased to 1.22 m (4.0 ft) in the transverse direction to accommodate high transverse shear forces. Plan dimensions at the bottom of the columns are 8.84 m (29 ft) in the longitudinal direction and 4.27 m (14 ft) in the transverse direction. The transverse dimension remains constant, but the longitudinal dimension tapers from 8.84 m (29 ft) at the bottom of the tower to 4.79 m (19 ft) at the very top of columns. Tower struts are provided with 1.52 m (5.0 ft) thick slabs and 1.07 m (3.5 ft) thick walls. All struts are 4.57 m (15 ft) wide with depths of 4.57, 6.10, and 7.62 m (15, 20, and 25 ft) respectively at the upper, middle, and lower struts. As shown in Figure 7, the struts break the tower column span into three bays. Beginning from the caisson pedestal, the spans of the tower columns between mid-depths of struts are 34, 60, and 45 m (111, 197, and 147 ft). Columns are conventionally reinforced, while the struts are post-tensioned and conventionally reinforced. Under the assumption that the elastic capacity of the towers would be exceeded, the struts were designed as “capacity-protected” members with location of plastic hinges restricted to tower columns. Column longitudinal reinforcement consists of #36 (#11) bars at 254 mm (10 in.) centers on each face of the column tower walls. This provides an approximately consistent reinforcement percentage of 1.4% throughout the tower columns.

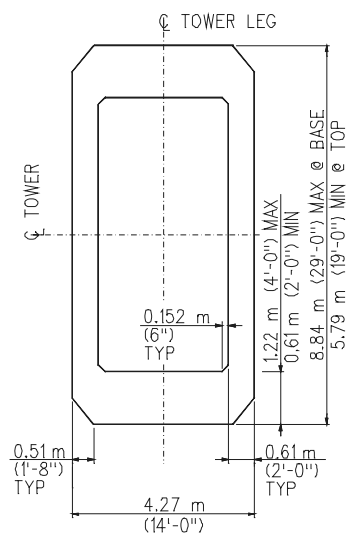


Figure 8 – Tower Section

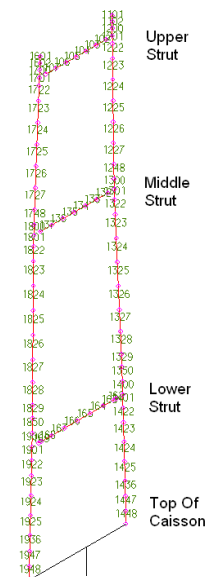


Figure 7
Discretization
plan of West
Tower

Criteria allowed repairable damage to the towers, which permitted the towers to respond beyond their elastic capacity and form plastic hinges. Potential plastic hinges are accommodated in seismic models by using moment-curvature elements with a plastic multi-linear material model. Input of this element type within the ADINA finite element software requires moment-curvature relationships for a full continuum of possible axial loads. Figure 9 provides moment-curvature plots for a typical tower section with axial loads varying from 44,500 kN (10,000 kips) to 267,000 kN (60,000 kips). Actual moment-curvature relationships used in models contained a wider spectrum of axial loads and were calculated by “Xtract” [6], a computer program specifically developed to determine moment-curvature relationships for reinforced-concrete sections. Also plotted on Figure 9 is the initial elastic stiffness selected for input into ADINA

moment-curvature elements. Selection of the slope and yield point of this line was dependent on whether tension, or compression, controlled at first yielding of the section. If tension controlled, selection of the slope and yield point coincides with the first yield of reinforcement, as determined by Xtract. When compression controlled, the slope and yield point were selected when concrete stress reached 60% of the ultimate confined concrete stress. This elastic stiffness is equivalent to the stiffness provided by approximately 30% of the gross moment of inertia of tower columns under axial dead load. Moment-curvature elements were implemented above the caisson pedestal and below the upper strut, and above and below the middle and lower strut, which represents all potential plastic hinge locations.

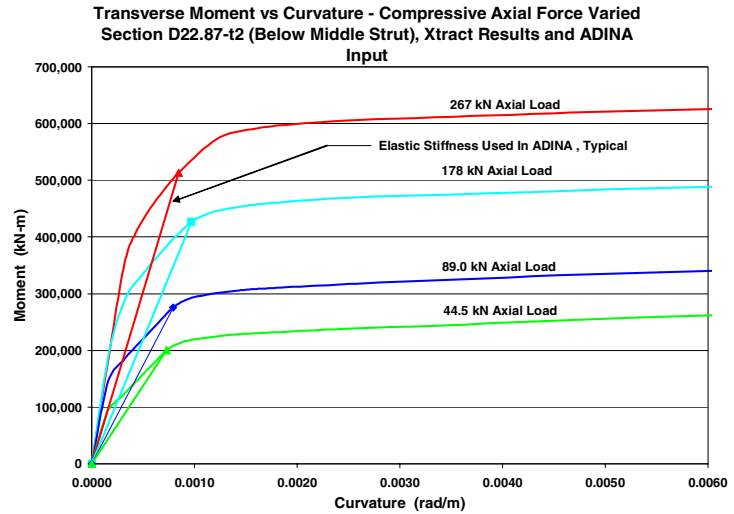


Figure 9 – Typical tower movement-curvature plots for varying axial loads

The material model used for moment-curvature elements is very similar to the material model used for Winkler soil springs depicted in Figure 6, with the exception that the model supports both tension and compression stresses. During loading and unloading beyond the initial yield point, strain hardening as well as hysteretic damping will occur.

Elastic elements were used for all of the other tower elements with an effective stiffness equal to one-half the gross stiffness used for these elastic elements to reflect softening of the columns after cracking. Full stiffness was used for the tower struts since these members are post-tensioned and remained elastic.

SUPERSTRUCTURE MODELING

Elastic elements were used throughout the superstructure. Beam elements were used for all members of the stiffening truss, floor beams, and secondary bracing. Truss elements were used for suspenders. Main suspension cables were modeled with beam elements, with very low stiffness which reflected the summation of the stiffness of individual wires under the assumption that slip was possible between wires. A detailed view of model discretization is shown in Figure 10. Floor beams had a nominal spacing of 6.1 m (20 ft), while suspenders were placed at every-other floor beam for a nominal spacing of 12.2 m (40 ft). Typical floor beam web depth varied from 1.68 m (5.5 ft) at the center of the bridge, to 1.07 m (3.5 ft) at the center line of the stiffening trusses. Suspenders consist of two, 41 mm (1½ in.) diameter wire ropes, except for the first 10 suspenders at each end of the bridge where the diameter was increased to 51 mm (1⅞-in.). The main suspension cable has a nominal diameter of 0.52 m (20½ in.) and is made up of 19 strands with 464 wires per strand for a total area of 0.17 m² (266 in²). Details of a typical floor beam and orthotropic deck are shown in Figure 11.

The orthotropic deck was represented in the model with shell elements. As shown in Figure 11, the orthotropic deck is composed of a 16 mm (⅝-in.) thick deck plate and 0.30 m (12-in.) deep stiffening ribs. It was recognized that using shell elements for deck modeling could not simultaneously capture precise deck stiffness in the two principle orthogonal directions of the deck. In the longitudinal direction, the deck plate and longitudinal stiffening ribs contribute to the axial, flexural, and in-plane diaphragm stiffness of the deck. In the transverse direction, only the deck plate will provide axial, flexural, and in-plane

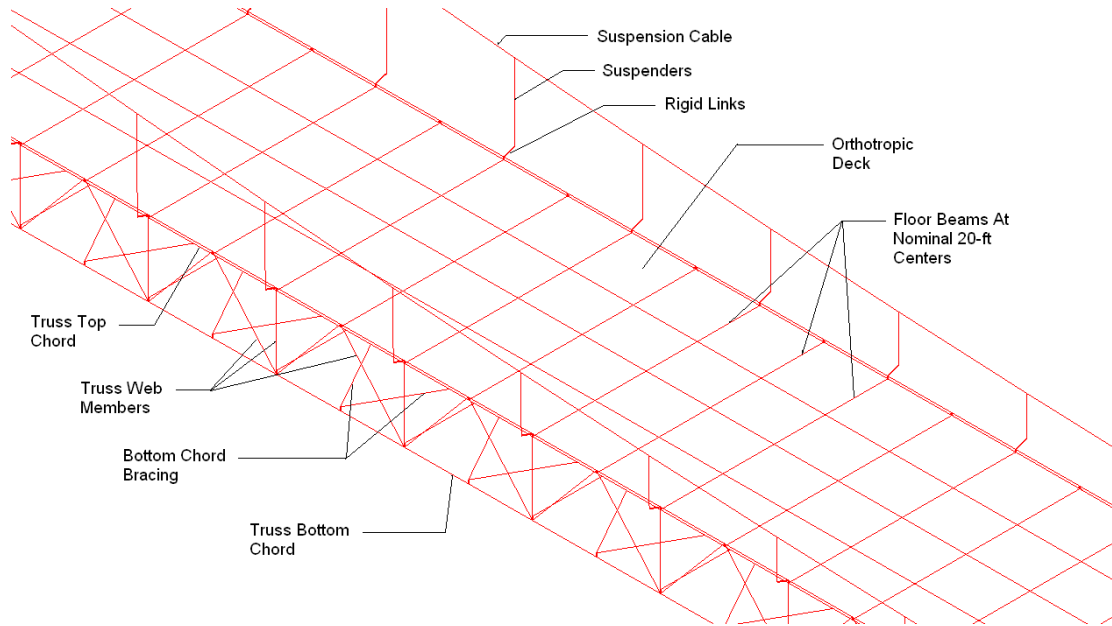


Figure 10 – Superstructure model discretization

diaphragm stiffness of the deck. Properties of deck shell elements were chosen to correctly reflect the stiffness of the orthotropic deck in the longitudinal direction. The thickness and modulus of elasticity of the shell element was adjusted to replicate the actual axial and flexural stiffness of the orthotropic deck in the longitudinal direction. Since the in-plane diaphragm stiffness is also proportional to thickness and modulus of elasticity, the proper diaphragm stiffness was also provided in the longitudinal direction of the bridge.

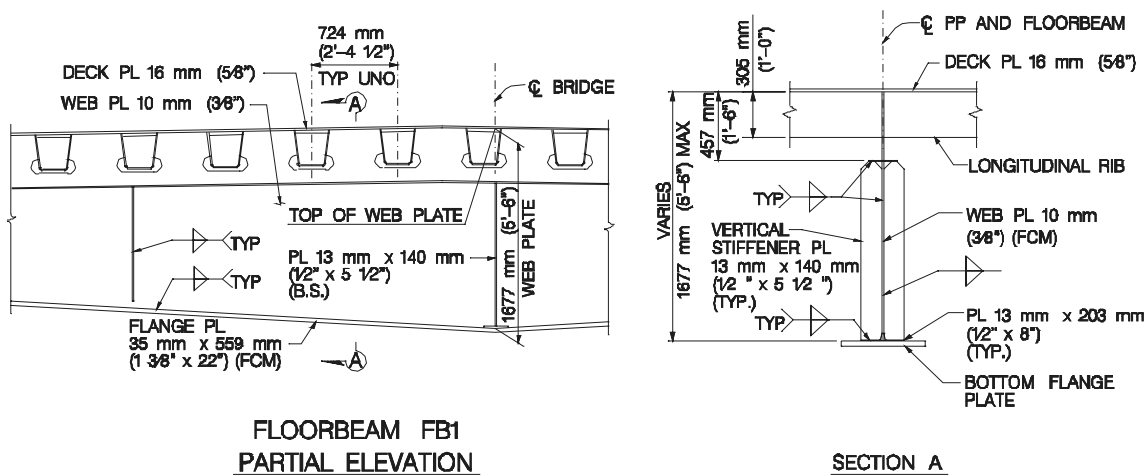


Figure 11 – Orthotropic deck details

To select deck shell element properties, the following two relationships are first recognized:

Equation 1 Deck Flexural Stiffness $\approx E_o I_o / L^n$

Equation 2 Deck Axial Stiffness $\approx E_o A_o / L$

Where: E_o = Young's Modulus for Orthotropic Deck
 L = Length
 I_o = Stiffness of Typical Orthotropic Deck Section
 A_o = Area of Typical Orthotropic Deck Section

The following stiffness relationships were then set:

Equation 3 Orthotropic Deck Flexural Stiffness, $E_o I_o$ = Shell Element Flexural Stiffness, $E_s b d_s^3 / 12$

Equation 4 Orthotropic Deck Axial Stiffness, $E_o A_o$ = Shell Element Axial Stiffness, $E_s b d_s$

Where: E_s = Young's Modulus for Equivalent Shell Elements
 b = Unit Width of Deck Shell Element and Orthotropic Deck
 d_s = Depth of Deck Shell Element

After determining the orthotropic deck flexural and axial stiffness, Equations 3 and 4 were used to evaluate the equivalent thickness, d_s , and Young's modulus, E_s , of deck shell elements. The resulting selected properties for deck shell elements were a thickness of 0.37 m (1.22 ft) and a Young's modulus of 13,170 MPa (1,910 ksi). Density of the shell elements was chosen to provide the proper mass of the structure. Since superstructure elements such as barriers, utilities, and maintenance appurtenances were not directly modeled, the selected shell element density was adjusted to account for these miscellaneous items.

Selecting deck stiffness by this procedure overstated deck axial, flexural and in-plane diaphragm stiffness in the transverse direction of the deck since the orthotropic ribs are not effective in the transverse direction. Deck flexural stiffness in the transverse direction is of minimal importance since the deck spans in the longitudinal direction. Although the deck shell elements used in models can span both longitudinally and transversely, the longitudinal floor beam spacing is 6.1 m (20 ft) versus a transverse spacing of 21.6 m (71 ft) for the stiffening trusses. At a 3.6:1 span aspect ratio, most loading from the deck shell elements will span between floor beams, similar to the actual orthotropic deck. To determine the consequence of using a greater transverse deck stiffness on the axial and in-plane diaphragm stiffness, a parametric study was performed. The axial and in-plane diaphragm stiffness was adjusted by reducing Young's modulus of deck shell elements by approximately 35% to reflect the ineffective stiffness of the orthotropic ribs in the transverse direction. Typical results of the analysis are shown in Figure 12, which compares top of tower displacement for a typical analysis case. Analyses results are essentially identical for the first 40 seconds of the analysis. As the tower softens during the last half of the time-history analysis, due to non-linear effects in towers, minor response differences become visible. However, these minor differences do not have a significant effect on analysis results.

DAMPING

Rayleigh damping was used for the entire model to approximate equivalent viscous damping. Specifying Rayleigh damping within the ADINA software requires entering two parameters – Rayleigh mass and stiffness proportional damping coefficients. Different coefficients may be entered for different portions of a structure. This option provided the opportunity to vary effective damping between the superstructure, towers and caissons. Selected Rayleigh damping is summarized in Figure 13. Recognizing that lower damping will occur in the steel superstructure with essentially elastic behavior, damping was set to vary between 2 and 5%. Since Criteria allowed repairable damage at towers and recognizing damping is typically higher in concrete structures, damping at towers was set between 4 and 5%.

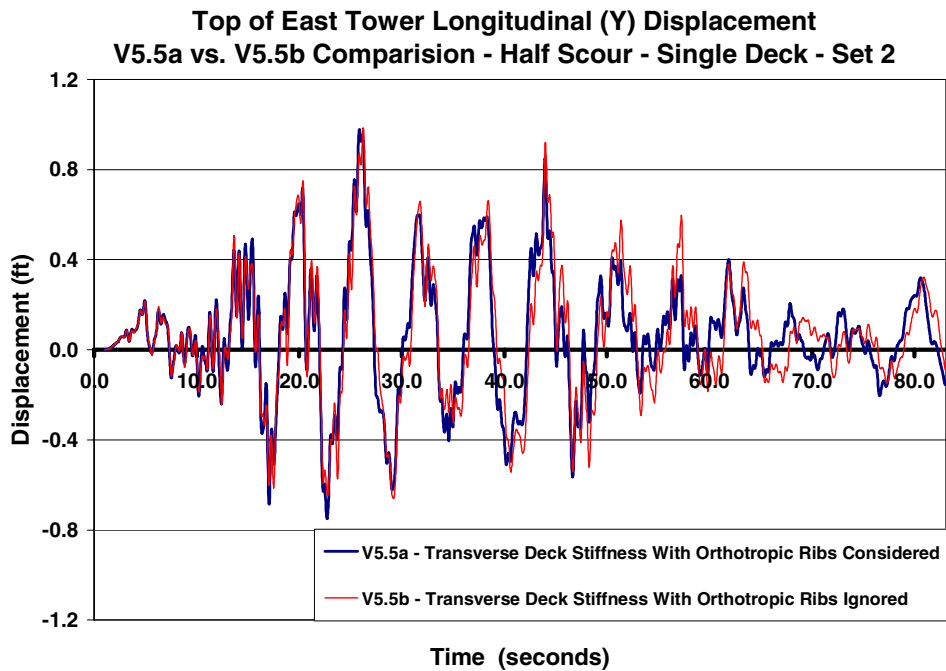


Figure 12 – Effect of alternate orthotropic deck stiffness on transverse top of east tower displacements

The last significant source of damping in the model is provided at discrete tower column locations that are expected to experience significant plastic deformation. Moment-curvature elements were implemented in the model at tower column locations where plastic hinges are anticipated. Additional damping may occur in these elements through hysteretic damping if these tower elements experience significant plastic deformation. Rayleigh damping was eliminated from any moment-curvature element determined to have significant plastic deformation.

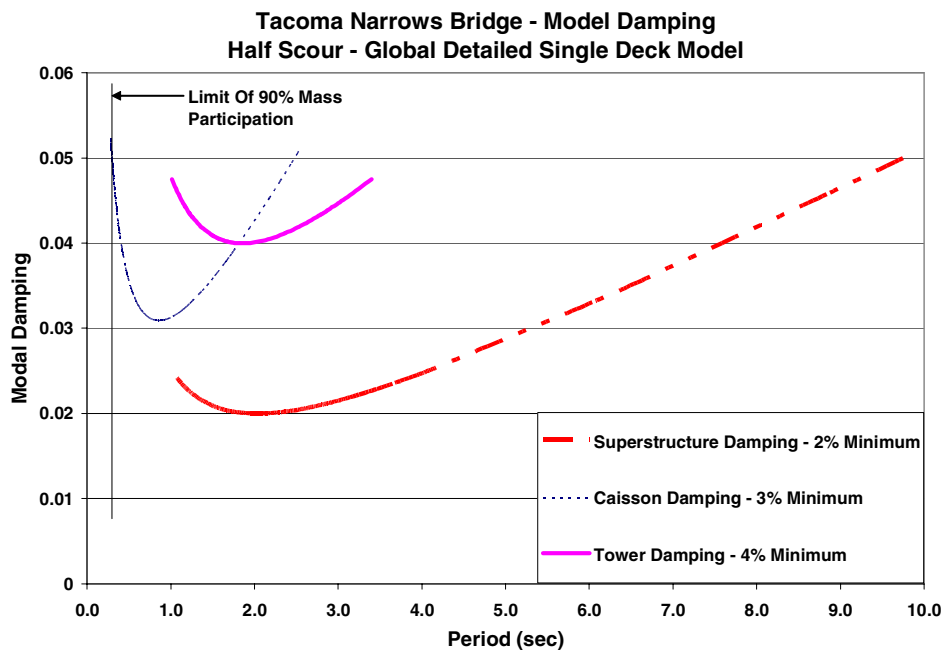


Figure 13 – Global model damping by bridge component

CAISSON PERFORMANCE

Figure 14 provides a typical time-history analysis record of the displacements at the top of the west caisson. Since Criteria stipulated caissons should have minimum damage, design of caisson consisted of providing sufficient reinforcement to resist all section forces determined from a number of seismic analyses. Since there is always uncertainty selecting appropriate soil properties when performing soil-structure interaction analysis, a number of bounding soil properties were determined and then an array of analyses performed to ensure the selection of upper bound caisson design forces. This resulted in using 36 seismic load cases for determining maximum caisson design forces. These 36 load cases were derived by combining three SEE ground motions, considering scour or no-scour, considering a single or double deck superstructure, and using three stiffness estimates of Winkler soil springs. Winkler soil spring stiffness was varied by increasing and decreasing—by 50%—the best-estimate of spring stiffness.

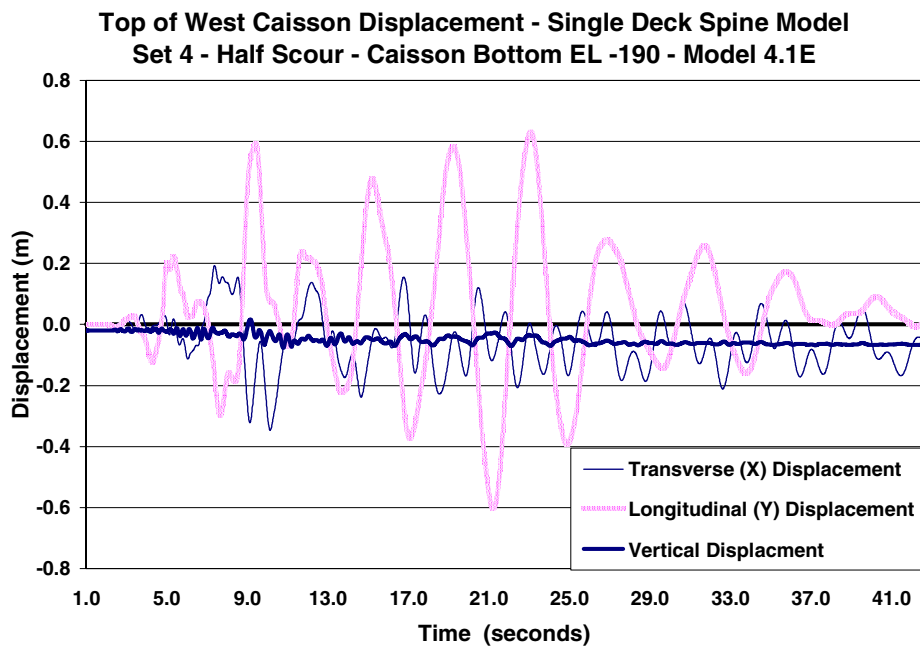


Figure 14 – Displacement time-history at top of West Caisson

For all of the load cases, caisson uplift from rocking was occurring and effectively serving as a fuse to reduce caisson forces. Verification that uplift occurred is illustrated by Figure 15, which provides a time-history plot of the displacement of the ground node below a corner of the east caisson and at the corner node of the caisson itself. In this figure, the heavy lower line represents the resulting profile of the ground below the caisson. The lighter upper line represents the response of the caisson bottom. When the two lines are in contact, the caisson is in contact with supporting ground. When the lines separate, the caisson has uplifted from supporting ground. Note that at a time of 1.0 second, which corresponds to the application of caisson dead load only, the caisson has settled approximately 15 mm (0.05 ft). Further inspection of Figure 15 shows a residual ground displacement at the end of the ground-motion of 0.09 m (0.30 ft) and maximum caisson uplift relative to the ground profile of 0.17 m (0.55 ft). By following the profile of the heavy lower line, the complete time-history of elastic rebound as well as residual settlement of supporting soil can be traced.

In addition to obtaining caisson section forces, caisson residual displacements were obtained from the 36 analyses and were found to comply with the criteria specified 0.30 m (1.0 ft) maximum limit, and were generally less than 0.15 m (0.5 ft). From Figure 14, it can be seen that this particular analysis resulted in residual displacements of approximately 75 mm (3 in.) in both the transverse and longitudinal directions.

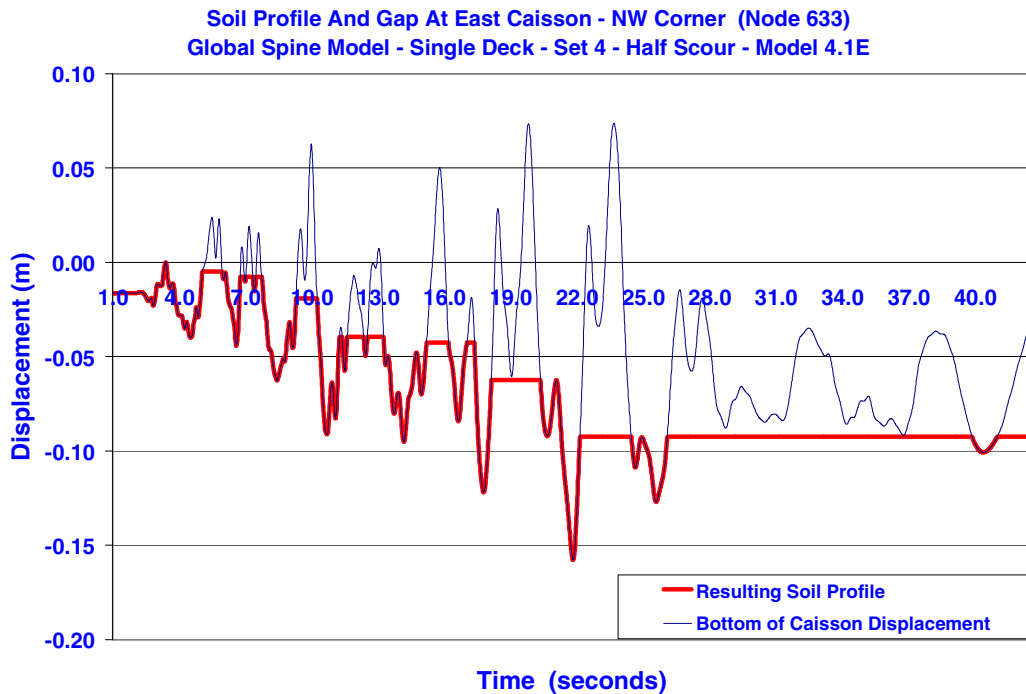


Figure 15 – Time history displacement of caisson and supporting ground at north-west corner of East Caisson

Caisson residual and peak displacements were generally attributed to caisson rotation, as maximum sliding displacements were 25 mm (1 in.) or less. This performance is attributed to the design philosophy adopted for caissons. Recognizing that during caissons rocking gravity acts as a restoring force whereas a similar restoring force is not present during sliding, caissons were embedded with sufficient depth into glacial till to minimize sliding potential.

TOWER PERFORMANCE

Criteria allowed repairable damage at towers, which permitted tower elements to respond beyond their elastic capacity, provided limits on maximum strain and residual displacement were met. Time-history analysis indicated that the elastic capacity of tower elements would be exceeded at some locations. In the transverse direction, towers consist of a three-story frame and transverse yielding of tower columns was generally restricted to the middle story. In the longitudinal direction, tower columns receive support from the caisson at the bottom of towers and the suspension cable at the top of towers. The great stiffness of caissons provides a fixed boundary condition at the bottom of tower columns. A pinned condition, with some longitudinal translation, is provided by the suspension cable saddle at the top of towers. Analysis indicated longitudinal plastic hinges would occur at the bottom of tower columns, directly above caisson pedestals. A second hinge also occurred near, or slightly above, the middle strut.

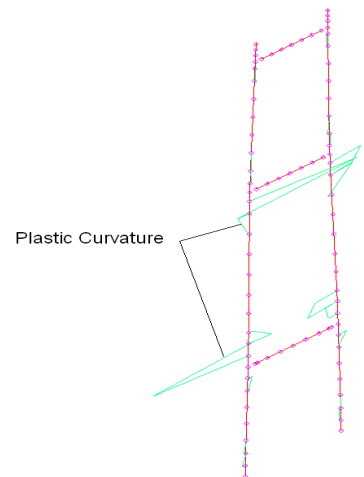


Figure 16 – Tower plastic curvature shown concentrated at middle story

Figure 16 provides a graphic representation of maximum plastic curvature demands at plastic hinge locations in the transverse direction of the west tower, for a typical seismic analysis. Note high curvatures occur

in the middle story, while very low plastic curvature demands occur in the upper and lower stories. Residual displacements occurring at the top of towers were also generated almost exclusively from rotations occurring in this story. This is a consequence of the proportions of the three stories. With a span of 60 m (197 ft), the middle story span significantly exceeds the spans of the lower and upper story spans of 34 m (111 ft) and 45 m (147 ft) respectively.

The seismic performance of towers is summarized in Figure 17, which compares maximum residual drift and strain demands against allowable limits for twelve SEE analyses cases. The twelve cases included combinations of the three SEE ground motions, single and double deck models, and with and without caisson half-scour. As seen in Figure 17, tower design was generally controlled by drift limits, not material strains, and transverse response was usually more critical than longitudinal response.

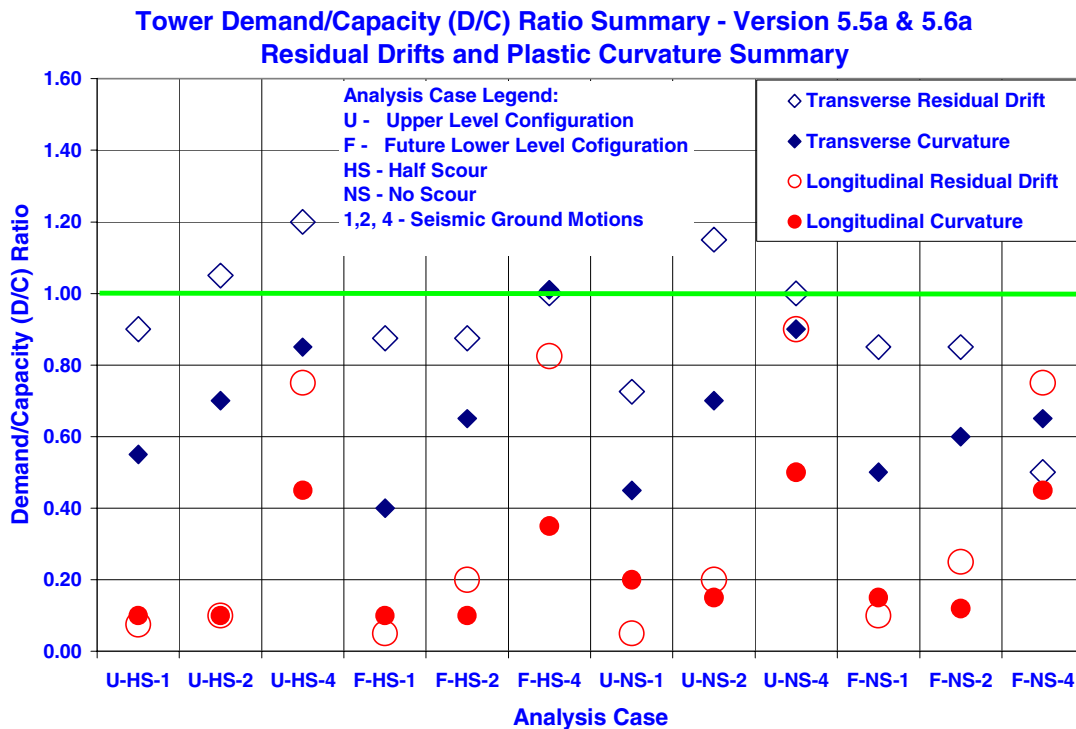


Figure 17 – Tower drift and strain demand/capacity summary

SUPERSTRUCTURE ANALYSIS RESULTS

Criteria specified no damage should occur for primary members of the stiffening truss and cable suspension system and allowed a maximum main cable direct tension stress of 689 MPa (100 ksi) under service conditions. Maximum dead load and seismic cable stresses peaked at 745 MPa (108 ksi), only slightly exceeding the maximum service load stress. Suspenders also performed well, with the minimum required safety factor of 2.0 or higher provided under combined seismic and dead loads.

Seismic force Demand/Capacity (D/C) ratios for primary stiffening truss members generally did not exceed a value of 1.0, except for a few isolated locations. These members were strengthened to provide a D/C ratio of 1.0 or less. Criteria allowed repairable damage for secondary stiffening truss members. Seismic D/C ratio values were acceptable for all secondary members.

CONCLUSIONS

Performance-based design criteria were successfully used to design the new Tacoma Narrows Suspension Bridge utilizing the design-build delivery method. Based on this experience, the following can be concluded:

- Performance-based seismic goals are readily achievable through analysis techniques that are currently available. By specifying performance-based goals through project specific design criteria, alternate levels of seismic performance versus cost can be achieved.
- For the new Tacoma Narrows Bridge, limits on residual drift at towers were more difficult to achieve than strain limits. The drift limit between the top and bottom of towers was limited to 0.41% and the concrete strain was limited to 75% of the ultimate allowable. Longitudinal reinforcement and transverse confinement reinforcement strain were limited respectively to 56% and 42% of ultimate allowable strain. Analyses showed that when towers minimally complied with residual drift limits, maximum strains were at approximately 70% of allowable limits. Although residual drift limits are not typically specified in bridge design codes, further research into the correlation of strain and drift limits is recommended.
- When it is important or desirable to control drift limits of towers in long-span bridges, inter-story drift limits should be specified in addition to total tower drift. While the total drift of the new Tacoma Narrows Bridge towers was 0.41%, this drift was primarily concentrated in the second story. When applied to the second story only, the 0.61 m residual drift limit results in an inter-story drift of 1.0%. For the new Tacoma Narrows Bridge, an inter-story drift of 1% was still more stringent than material strain limits. However, specifying inter-story residual drift limits for multi-story towers of long-span bridges would prevent excessive deformations from occurring in a limited number of stories and provide the desired effect of distributing plastic deformations throughout the tower.
- Since rocking of large deep water caissons is an effective fusing mechanism, soil-structure analysis techniques should be used that permit this response while also verify the stability of the structure during rocking.
- The new Tacoma Narrows Bridge superstructure did not receive significant seismic demands. The suspension system designed for service loads was adequate for seismic demands. However, limited and selected strengthening of the stiffening truss was required to ensure all primary members remained elastic during seismic loading as required by design criteria.

ACKNOWLEDGEMENTS

The authors wish to thank and acknowledge the many other participants in this project. The Washington State Department of Transportation (WSDOT) is the owner of the bridge and is providing oversight for both the design and construction. The bridge is being built by Tacoma Narrows Constructors (TNC), a joint venture of the Bechtel Corp. and Peter Kiewit Sons', Inc. TNC hired a joint venture of Parson Corporation and HNTB Corporation to perform engineering services during design and construction of the bridge.

REFERENCES

1. Washington Department of Transportation. "Bridge Design Manual", Program Development Division, Bridge and Structures, Olympia, Washington, 1998.
2. ADINA, Version 7.5.4. "Automatic Dynamic Incremental Nonlinear Analysis", ADINA R & D, Inc., Watertown, Massachusetts, 2002.

3. Goyal, A. and Chopra, A. K. "Simplified Evaluation of Added Hydrodynamic Mass for Intake Towers", Journal of Engineering Mechanics, American Society of Civil Engineers, July, 1989, 1393-1412.
4. Lam, P. "Interim Report – Tacoma Narrows Bridge, Pseudo-Static Back Substitution Round-3 SSI (65% Design Submittal)", December 19, 2002.
5. Lam, P. "Final Soil-Structure Interaction Report for Tacoma Narrows Bridge, Caisson Response", April 7, 2003.
6. Xtract, Version 2.6.2. "Cross-Sectional Structural Analysis of Components", Imbsen Software Systems, Sacramento, California, 2002.